ACS Catalysis

Research Article

pubs.acs.org/acscatalysis

Active Oxygen Vacancy Site for Methanol Synthesis from CO_2 Hydrogenation on In_2O_3(110): A DFT Study

Jingyun Ye,[†,‡] Changjun Liu,[†] Donghai Mei,[§] and Qingfeng Ge*[,†,‡]

[†]School of Chemical Engineering and Technology, Tianjin University, Tianjin 300072, China

[‡]Department of Chemistry and Biochemistry, Southern Illinois University, Carbondale, Illinois 62901, United States

[§]Institute for Integrated Catalysis, Pacific Northwest National Laboratory, Richland, Washington 99352, United States

Supporting Information

ABSTRACT: Methanol synthesis from CO_2 hydrogenation on the defective In_2O_3(110) surface with surface oxygen vacancies has been investigated using periodic density functional theory calculations. The relative stabilities of six possible surface oxygen vacancies numbered from O_{v1} to O_{v6} on the perfect In_2O_3(110) surface were examined. The calculated oxygen vacancy formation energies show that the D1 surface with the O_{v1} defective site is the most thermodynamically favorable while the D4 surface with the O_{v4} defective site is the least stable. Two different methanol synthesis routes from CO_2 hydrogenation over both D1 and D4 surfaces were studied, and the D4 surface was found to be more favorable for CO_2 activation and hydrogenation. On the D4 surface, one of the O atoms of the CO_2 molecule fills in the O_{v4} site upon adsorption. Hydrogenation of CO_2 to HCOO on the D4 surface is both thermodynamically and kinetically favorable. Further hydrogenation of HCOO involves both forming the C−H bond and breaking the C−O bond, resulting in H_2CO and hydroxyl. The HCOO hydrogenation is slightly endothermic with an activation barrier of 0.57 eV. A high barrier of 1.14 eV for the hydrogenation of H_2CO to H_3CO indicates that this step is the rate-limiting step in the methanol synthesis on the defective In_2O_3(110) surface.

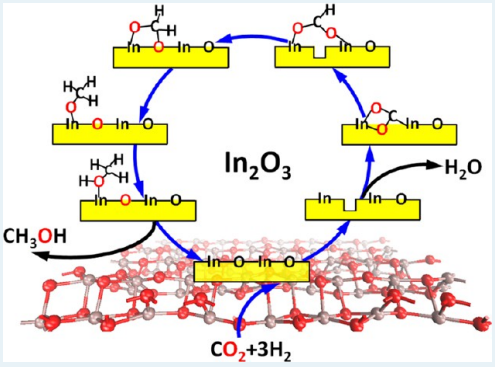

KEYWORDS: *catalytic CO_2 hydrogenation, methanol synthesis, defective In_2O_3 surface, oxygen vacancy, density functional theory*

1. INTRODUCTION

Catalytic conversion of CO_2 to methanol via hydrogenation has attracted enormous interest for its central role in CO_2 utilization using heterogeneous catalysts.[1−3] Methanol can be used not only as the starting feedstock for many other useful chemicals but also as an alternative source in the production of liquid fuels. Currently, methanol is industrially synthesized from syngas (CO_2/CO/H_2) at 493−573 K and 5−10 MPa using a Cu/ZnO/Al_2O_3 catalyst.[4] Due to the high activity of Cu, CO_2 hydrogenation for methanol synthesis has been extensively studied on Cu-based catalysts through both experiments[5−9] and theory.[10−15] Three reaction pathways had been proposed.[13−15] In the formate (HCOO) route, CO_2 is first hydrogenated to HCOO. This is followed by HCOO hydrogenation to dioxymethylene (H_2COO), and further hydrogenation to methoxy (H_3CO), and then the final product, methanol (CH_3OH). The hydrogenation of HCOO to H_2CO was assumed to be the rate-limiting step in the formate route.[16] The second reaction route involves the reverse water gas shift (RWGS) reaction ($CO_2 + H_2 \rightarrow CO + H_2O$). CO_2 is first reduced to CO, which is then consecutively hydrogenated to methanol. The last route is via the hydrocarboxyl (COOH) species. Instead of the HCOO species, CO_2 is initially protonated to the COOH. Then, the COOH is converted to COHOH, which decomposes to COH and OH. The methanol is generated by the hydrogenation of COH.[13]

Compared with numerous studies on the metal catalysts, few studies on metal oxide have been reported.[17−19] Kiss et al.[17] found that different charge states of oxygen vacancy defects (F centers) on the defective ZnO(0001) surface play important roles in determining the reaction intermediates and reaction pathways for CO hydrogenation to methanol. At the defective F^- site, methanol is favorably produced via the hydroxymethyl (H_2COH) rather than via the methoxy (H_3CO) species. Zhao et al. studied methanol synthesis from CO_2 or CO on the Zn-terminated ZnO(0001)[18] and suggested that CO is the carbon source of methanol. Recently, the unique catalytic properties of In_2O_3 have attracted a lot of attention.[20−22] Umegaki et al. reported a high CO_2 selectivity without CO impurity in ethanol steam reforming over a worm-like In_2O_3 catalyst.[23] These authors speculated that the high CO_2 selectivity is a result of the suppressed reverse water-gas shift (RWGS) reaction in the presence of In_2O_3. Similarly, Lorenz et al. reported an almost 100% CO_2 selectivity in methanol steam reforming using a pure In_2O_3 catalyst.[21] The reason for a high CO_2 selectivity and

Received: February 19, 2013
Revised: April 29, 2013
Published: May 2, 2013

   dx.doi.org/10.1021/cs400132a | ACS Catal. 2013, 3, 1296−1306

resistance toward CO production on In_2O_3 is further demonstrated by Bielz et al. who found that CO can easily reduce the In_2O_3, while CO_2 could not replenish the oxygen vacancy.[22] The unique redox property of In_2O_3 leads to a high CO_2 selectivity in methanol steam reforming (MSR). For methanol synthesis from CO_2 hydrogenation, the reverse reaction of MSR, the ultimate goal is to use CO_2, replacing CO as the only carbon source, to produce methanol by using highly selective catalysts. Previously experimental results suggested that the high CO_2 selectivity and strong resistance of the oxygen defective In_2O_3 catalyst to RWGS[24,25] made the In_2O_3 an attractive candidate for methanol synthesis from CO_2 hydrogenation.

Previously, we studied CO_2 adsorption and the initial steps of hydrogenation on the perfect $In_2O_3(110)$ surface using density functional theory (DFT).[26] Herein, we examine the creation of oxygen vacancies on the In_2O_3 surface and its impact on methanol synthesis from CO_2 hydrogenation. This work was organized as follows: we first examined the relative stability of different surface oxygen vacancy sites on $In_2O_3(110)$ and then compared two extremes of oxygen vacancy sites for CO_2 hydrogenation. Finally, we chose the most active oxygen vacancy site and mapped out the pathways for CO_2 hydrogenation to methanol.

2. COMPUTATIONAL DETAILS

All the calculations were performed using the Vienna ab initio simulation package (VASP),[27−29] a periodic DFT code with projector augmented wave (PAW) potentials. The nonlocal exchange correlation energy was evaluated using the Perdew−Burke−Ernzerhof functional.[30] The semicore 5s and 5p states of In were treated explicitly as valence states within the scalar-relativistic PAW approach.[31] A plane wave basis set with a cutoff energy of 400 eV and a $(2 \times 2 \times 1)$ k-point grid generated with the Monkhorst−Pack scheme were found to give converged results. The atomic structures were relaxed using either the conjugate gradient algorithm or the quasi-Newton scheme as implemented in the VASP code until the forces on all unconstrained atoms were ≤0.03 eV/Å.

The perfect $In_2O_3(110)$ surface is modeled with a $(1\times\sqrt{2})$ supercell, built from the optimized In_2O_3 bulk unit cell with a lattice parameter $a = b = c = 10.18$ Å.[26] The supercell has a dimension of 10.18 Å × 14.40 Å × 17.96 Å. The surface slab consists of 48 O atoms and 32 In atoms, distributed in four atomic layers and separated by a vacuum of 10 Å. The oxygen vacancy on the $In_2O_3(110)$ surface was created by removing one surface O atom from the perfect $In_2O_3(110)$ surface. In all calculations, the bottom two layers were frozen at their equilibrium bulk positions, whereas the top two layers together with the adsorbates were allowed to relax. The adsorption energies of adsorbates were defined as

$$E_{ad}(M) = E_{M/S} - E_S - E_M$$

where M represents adsorbate and S represents the perfect $In_2O_3(110)$ surface or the defective $In_2O_3(110)$ surface with one oxygen vacancy. In the following discussion, we denote the perfect $In_2O_3(110)$ surface and the defective $In_2O_3(110)$ surface as P and D, respectively. $E_{M/S}$, E_S, and E_M represent the total energies of the surface slab with the adsorbates, the clean optimized P or D surface slabs, and an isolated molecule (radical), respectively. According to the above definition, a negative value indicates the process is exothermic, whereas positive values are endothermic. Bader charge analyses[32,33] were performed for perfect, oxygen defective In_2O_3 (110) surface, and defective surface with CO_2 adsorption. Transition states along a reaction pathway were determined in two steps: First, the nudged elastic band method[34] typically with seven to nine images was used to locate the likely transition state. Second, the likely transition state was relaxed using the quasi-Newton algorithm with the same force convergence criterion. The finally relaxed transition state was confirmed through frequency analysis. All the atoms allowed to relax were included in the frequency analysis of the transition state.

3. RESULTS AND DISCUSSION

3.1. Oxygen Vacancy Creation on the $In_2O_3(110)$ Surface. The perfect $In_2O_3(110)$ surface is shown in Figure 1a. The surface consists of In−O−In chains, and each chain consists of two O−In squares connected by a short $O_3-In_3-O_4$ segment symmetrically with respect to In_3.[26] The defective $In_2O_3(110)$ surface with an oxygen vacancy is created by removing one surface oxygen atom in turn from the optimized perfect $In_2O_3(110)$ surface. We examined all six possibilities of surface oxygen vacancy, denoted as O_{v1} to O_{v6}. Table 1 lists the reaction energy for oxygen vacancy creation by thermal desorption of lattice oxygen, as well as by H_2 and CO reduction. As shown in Table 1, oxygen vacancy creation is highly endothermic via direct thermal desorption, while it is exothermic with the assistance of H_2 or CO. Furthermore, our results also show that the creation of an oxygen vacancy is more exothermic using CO than H_2. This is consistent with the previous experimental observations[20,22] that the oxygen vacancy creation on the $In_2O_3(110)$ surface is more facile via the H_2 or CO reduction than through thermal desorption. The oxygen vacancy was reported to appear at ~673 K.[20] In contrast, the In_2O_3 surface reduction occurs at 293 K with CO and at 340 K with H_2, respectively.[22] The calculated reaction energies for oxygen vacancy creation on the $In_2O_3(110)$ surface indicate that oxygen vacancy at the O_{v1} site is easiest to generate while that at O_{v4} is the most difficult. Figure 1b shows two defective In_2O_3 (110) surfaces where an oxygen vacancy is at the O_{v1} or O_{v4} site, corresponding to the D1 or D4 surface, respectively. As shown in Figure 1b, the connectivity of the chain on the surface was maintained through $In_1-O_2-In_2$ after the O_{v1} vacancy site was created on the surface. In contrast, the creation of the O_{v4}

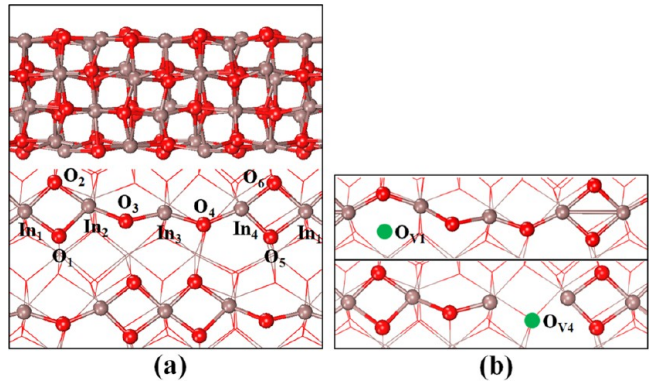

Figure 1. (a) Optimized structure of the $In_2O_3(110)$ surface, side view (upper) and top view (lower). (b) The D1 (upper) and D4 (lower) defective $In_2O_3(110)$ surfaces. Red, O atoms; brown, In atoms; green, O vacancy.

dx.doi.org/10.1021/cs400132a | ACS Catal. 2013, 3, 1296−1306

Table 1. Reaction Energies (in eV) of Oxygen Vacancy Creation on the $In_2O_3(110)$ Surface by Thermal Desorption and Reduction

		ΔE^a					
reaction	reaction equation	D1	D2	D3	D4	D5	D6
thermal desorption	P_In_2O_3(110) → Ov_In_2O_3(110) + 1/2 O_2	1.96	1.98	2.35	2.47	2.40	2.14
H_2 reduction	P_In_2O_3(110) + H_2 → Ov_In_2O_3(110) + H_2O	−0.57	−0.56	−0.19	−0.07	−0.13	−0.40
CO reduction	P_In_2O_3(110) + CO → Ov_In_2O_3(110) + CO_2	−1.30	−1.28	−0.91	−0.79	−0.86	−1.12

[a] ΔE is calculated as $(E_D + E_{oxi}) - (E_P + E_{red})$. E_{oxi} is the total energy of the oxidant ($^1/_2O_2$, H_2O, or CO_2) while E_{red} is the total energy of the reductant (H_2 or CO).

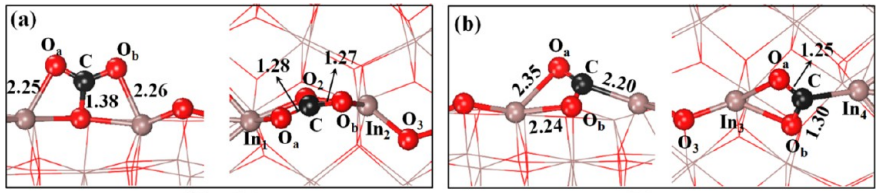

Figure 2. Optimized adsorption structures of CO_2 on the D1 and D4 defective $In_2O_3(110)$ surfaces.

Table 2. Atomic Bader Charges (in |e|) for CO_2 Adsorption on the Perfect and Defective $In_2O_3(110)$ Surfaces

charge	In_1	In_2	In_3	In_4	C	O_a	O_b	total surface In	total CO_2
P	+0.55	+0.56	+0.53	+0.51				+2.15	
D1	+0.42	+0.47	+0.50	+0.49				+1.88	
D4	+0.54	+0.55	+0.05	+0.10				+1.24	
CO_2					+2.12	−1.06	−1.06		0
CO_2_D1	+0.54	+0.56	+0.44	+0.50	+2.08	−1.11	−1.12		−0.15
CO_2_D4	+0.54	+0.55	+0.40	+0.54	+1.29	−1.07	−1.11		−0.89

vacancy site broke the connectivity of the chain structure on the surface. In the following, we will investigate methanol synthesis from CO_2 hydrogenation over the defective $In_2O_3(110)$ surfaces with the O_{v1} and the O_{v4} vacancies.

3.2. CO_2 Adsorption and Hydrogenation on Oxygen Defective $In_2O_3(110)$ Surfaces: D1 and D4. *3.2.1. CO_2 Adsorption.* The structures of CO_2 adsorption on the oxygen defective D1 and D4 surfaces are shown in Figure 2. For CO_2 adsorption on the D1 surface (denoted as CO_2_D1 for abbreviation), different initial structures with CO_2 insertion into the O_{1v} vacancy site were tested. We find none of those initial structures leads to a stable CO_2 adsorption configuration. Instead, CO_2 is bound at the surface O atom next to the O_{1v} site, forming a carbonate species (Figure 2a). The bond lengths of O_a−In_1, O_b−In_2, and C−O are 2.25 Å, 2.26 Å, and 1.38 Å, respectively. We note that both C−O bonds of the adsorbed CO_2 elongate to 1.28 Å and 1.27 Å from the optimized C−O bond length of 1.18 Å of a free CO_2 molecule.

CO_2 can adsorb at the O_{v4} site by inserting one of its O atoms in the vacancy site on the D4 surface (denoted as CO_2_D4 for abbreviation). In the CO_2_D4 structure shown in Figure 2b, the O_a and O_b atoms bind the In_3 atom and the C atom binds the In_4 atom. The bond lengths of O_a−In_3, O_b−In_3, and C−In_4 are 2.35 Å, 2.24 Å, and 2.20 Å, respectively. Similar C−O bond elongation to CO_2_D1 is found in the CO_2_D4 structure.

Our results show that the adsorption energy of CO_2 on the D1, and the D4 surfaces are very similar (−0.57 and −0.61 eV). These values are lower than the calculated adsorption energy of CO_2 on the perfect surface, which is about −1.25 eV.[26] However, we note a significant difference between the structures of the two surfaces with CO_2. On D1, adsorbed CO_2 interacts with the O atom next to the vacancy to form a carbonate structure, similar to that on the perfect surface. In contrast, adsorbed CO_2 on D4 fills in the vacancy. The existence of defects has been reported to promote CO_2 adsorption and activation on metal oxide surfaces.[35−37] Recent DFT studies also confirmed that CO_2 adsorbs at the oxygen vacancy site over the Zn-terminated ZnO(0001) surface by inserting one of the O atoms of CO_2 into the vacancy, forming a bent CO_2^- species.[36,37] However, on metal surfaces, including Cu(111)[13−15] and Ni(111),[38] CO_2 adsorbs weakly and is activated through an Eley−Rideal mechanism. Consequently, introducing metal oxides to a catalyst promotes CO_2 adsorption and activation.[39,40]

Our results also show that the energy penalty for replenishing the O_{v4} site with the adsorbed CO_2 is +1.40 eV, indicating that it is highly unlikely to generate CO from CO_2 by reacting with the defective In_2O_3 surface. To further confirm this, we performed *ab initio* molecular dynamics simulations by placing CO_2 in the vacancy site in the stable adsorption configuration (see the animation in the Supporting Information). The result showed no CO desorption at 800 K. Instead, CO_2 desorbs as a molecule from the CO_2_D4 surface at ∼0.5 ps. This result is in good agreement with the previous experimental observation that CO_2 can be formed from CO oxidation on the In_2O_3 surface, resulting in a reduced surface. However, the reversible process of repairing the reduced surface with CO_2 did not occur when the surface cooled down.[22]

To further characterize CO_2 adsorbed on the D1 and D4 surfaces, we performed Bader charge analyses for the perfect surface, the oxygen defective surface, and various CO_2 adsorption configurations and summarized the results in Table 2. The results show that the creation of the O_{v1} defective site reduces the charges on In_1 and In_2 to +0.42 |e| and +0.47 |e|, respectively. The charges on In_3 and In_4 remain nearly the same as those on the perfect surface. The creation of O_{v4} has a more pronounced effect on In_3 and In_4, reducing their charge to +0.05 |e| and +0.10 |e|,

dx.doi.org/10.1021/cs400132a | ACS Catal. 2013, 3, 1296−1306

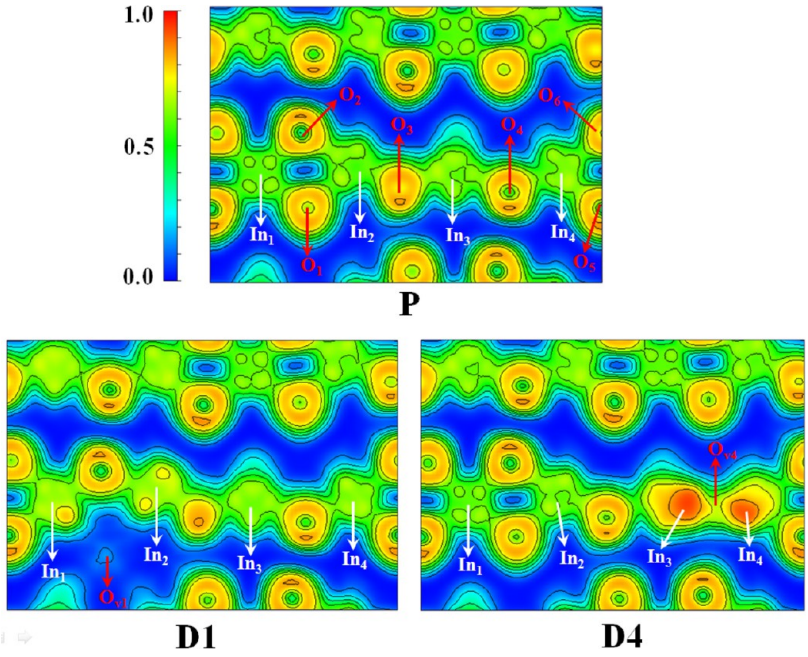

Figure 3. Electronic localization function contours of the perfect P, D1, and D4 surfaces.

respectively, but keeps the charges on In_1 and In_2 nearly the same as that on the perfect surface. The electronic localization function (ELF) contour maps of perfect and defective D1 and D4 surfaces are shown in Figure 3. The ELF maps clearly show that the ELF value is close to zero at the O_{v1} site on the D1 surface, indicating a highly delocalized electron distribution. In contrast, the creation of the O_{v4} vacancy makes the electron density highly localized on the neighboring In sites, indicated by the high ELF values at the In sites in D4 of Figure 3. The ELF map also shows that there is a degree of electron localization at the O_{v4} site on the D4 surface. The results reflect the fact that the creation of oxygen vacancy donates electrons to the surface, making the surface reduced and potentially electron donors. The results also indicate that D1 retains the characteristics of the perfect surface, while D4 is much more nucleophilic. The electron donating abilities of the two surfaces is also reflected in the charge gained by the adsorbed CO_2. The charge on adsorbed CO_2 in CO_2_D1 is −0.15 |*e*| and in CO_2_D4 is −0.89 |*e*|. The results show that the adsorbed CO_2 is much more reduced on D4 than on D1 by receiving more electrons. We also noted that the charge on the adsorbed CO_2 in CO_2_D1 is nearly the same as that on the perfect surface (−0.14 | *e*|),[26] indicating a similar electron donating ability of the D1 surface to that of the perfect surface. In contrast, the adsorbed CO_2 is more negatively charged on D4 than on D1.

3.2.2. CO_2 Hydrogenation and Protonation. In order to evaluate the activities of different oxygen vacancy sites for methanol synthesis from CO_2 hydrogenation, we tested CO_2 hydrogenation and protonation on the D1 and D4 surfaces. In the following discussion, we use "protonation" for hydrogen reacting with oxygen to form an O−H bond, whereas we use "hydrogenation" for hydrogen reacting with carbon to form a C−H bond.

Both CO_2 hydrogenation and protonation on the D1 surface were examined by adding a H adatom at the neighboring site of the adsorbed CO_2, forming $[CO_2+H_{In}]$* and $[CO_2+H_O]$*, as shown in Figure 4a. In $[CO_2+H_{In}]$*, the distance between the C atom of the adsorbed CO_2 and the H atom is 3.04 Å. The coadsorption energy is −0.07 eV. In the transition state (TS1), the H−In_1 bond is elongated to 2.37 Å as the H atom approaches the C atom at a distance of 1.71 Å. In the final state, the HCOO* species form on the surface with a single O_b−In_2 bond of 2.15 Å. Our result shows that hydrogenation of CO_2 to HCOO* on the D1 surface is endothermic by +0.38 eV with an activation barrier of 1.35 eV. CO_2 can also be protonated by the neighboring hydroxyl, i.e., $[CO_2+H_O]$*. This initial state is significantly more stable than the $[CO_2+H_{In}]$*, by ∼1.0 eV. The distance between the O_b atom of the adsorbed CO_2 and the H atom of the hydroxyl is 2.40 Å. In the transition state (TS2), the approaching H atom is in the middle of the two oxygen atoms with two O−H distances at 1.26 and 1.31 Å. CO_2 protonation on the D1 surface is endothermic by +0.58 eV with an activation barrier of 0.71 eV. However, we noted that the backward reaction, i.e. COOH* decomposition, is exothermic by −0.58 eV with an activation barrier of 0.13 eV, significantly more favorable than the forward reaction (CO_2 protonation).

For CO_2 hydrogenation on the D4 surface, we find that the adsorbed H atom at either In_3 or In_4 sites can react with the adsorbed CO_2, forming HCOO*. The adsorbed CO_2 goes through a configurational transformation before being hydrogenated. As the H atom approaches, the In_3−O_b bond is broken, and the adsorbed CO_2 with a linear structure binds In_3 with a single In−O_a bond, as shown in $[CO_2+H_{In}]$* of Figure 4b. The H atom then attacks the C atom and forms HCOO* in a monodentate structure. Our calculated reaction energy for the CO_2 hydrogenation on the D4 surface indicates that this step is slightly exothermic (−0.21 eV). The activation barrier is 0.15 eV. For CO_2 protonation, the H atom most likely comes from the hydroxyl on the neighboring row. The hydroxyl in the same row sits too far away from the adsorbed CO_2. As shown in Figure 4b, the $[CO_2+H_O]$* on the D4 surface is very stable with a coadsorption energy of −1.94 eV. The distance between the H atoms and the O_a atom is 2.04 Å. In transition state (TS2), the distances between H and the two O atoms are 1.69 Å and 1.76 Å. These distances are much larger than on the D1 surface. The result shows that the protonation of CO_2 is highly endothermic with a reaction energy of +1.39 eV. The barrier is also extremely

dx.doi.org/10.1021/cs400132a | *ACS Catal.* 2013, 3, 1296−1306

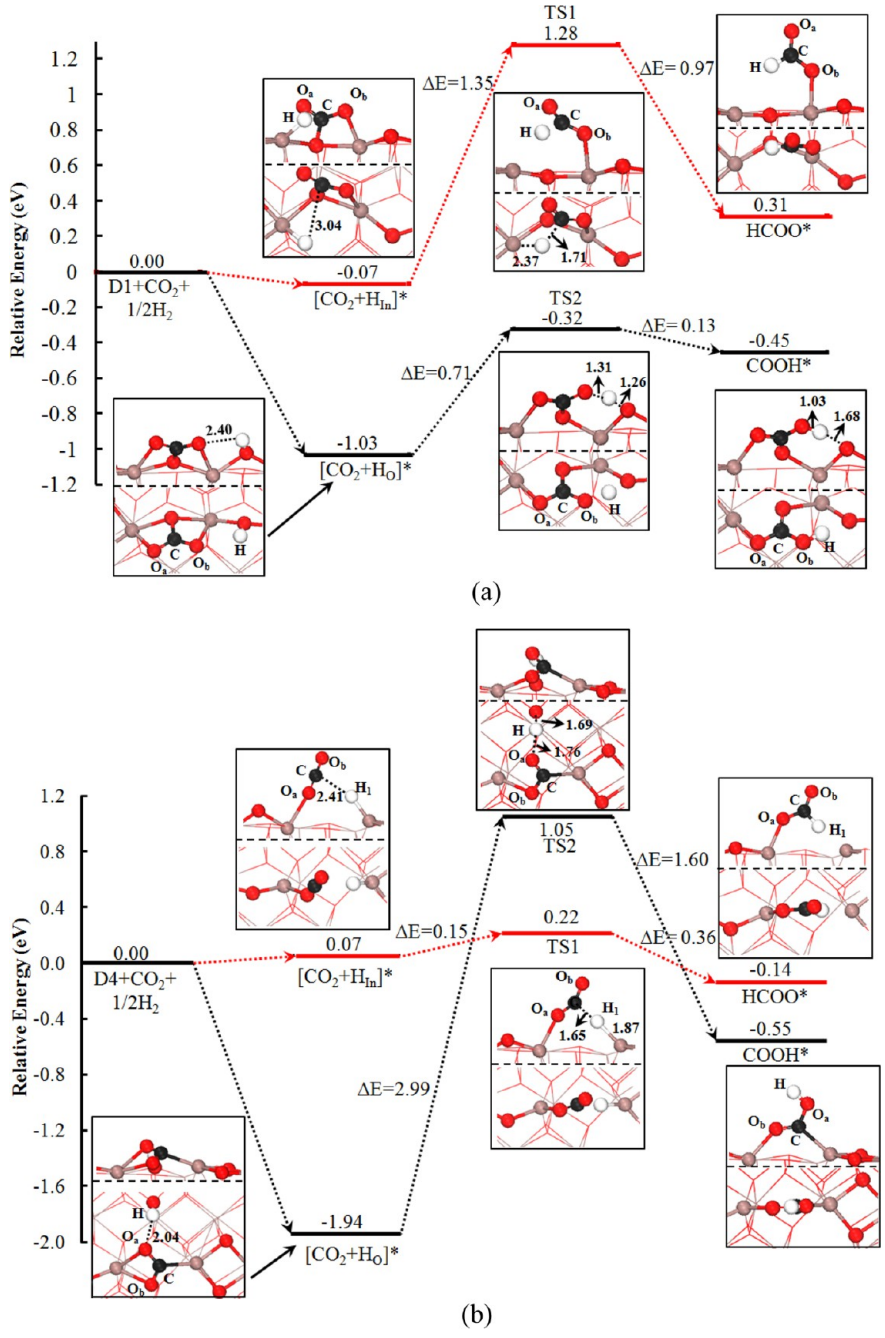

Figure 4. Potential energy profiles of CO_2 hydrogenation and protonation on the D1 (a) and the D4 (b) defective $In_2O_3(110)$ surfaces. Red line, hydrogenation; black line, protonation. A* represents the adsorption state of A on the surface, and [A+B]* represents the coadsorption state of A and B on the surface.

high (2.99 eV), indicating that the COOH* will not be produced on the D4 surface.

The hydrogenation and protonation of CO_2 are the initial steps for methanol formation. On the basis of the above results, we conclude that CO_2 protonation is both thermodynamically and kinetically more favorable than CO_2 hydrogenation on the D1 surface. This is similar to CO_2 adsorbed on the perfect surface where protonation is favorable over the hydrogenation.[26] However, hydrogenation of CO_2 is both thermodynamically and kinetically more favorable than CO_2 protonation on the D4 surface. Comparing the hydrogenation steps on the D1 and D4 surfaces, we find that CO_2 hydrogenation on the D4 surface has a significantly lower barrier (0.15 eV vs 1.35 eV) and is more exothermic (−0.21 eV vs +0.38 eV). On the perfect surface, the hydrogenation step is 0.33 eV endothermic and has a barrier of 0.65 eV.[26] Even though creating the D4 surface costs ∼0.5 eV more than creating the D1 surface, the low CO_2 hydrogenation barrier on D4 outweighs the higher vacancy creation energy. Consequently, the overall CO_2 hydrogenation turnover will dominantly occur on the D4 surface. This conclusion can be clearly seen from potential energy profiles shown in Figure 5, which includes vacancy creation on the perfect surface as well as the first and second CO_2 hydrogenation steps on both D1 and D4. As shown Figure 5, the activation barrier for the second CO_2 hydrogenation step on D4 is 0.97 eV lower than that on D1, and overall, CO_2 hydrogenation on D4 is energetically more

dx.doi.org/10.1021/cs400132a | ACS Catal. 2013, 3, 1296−1306

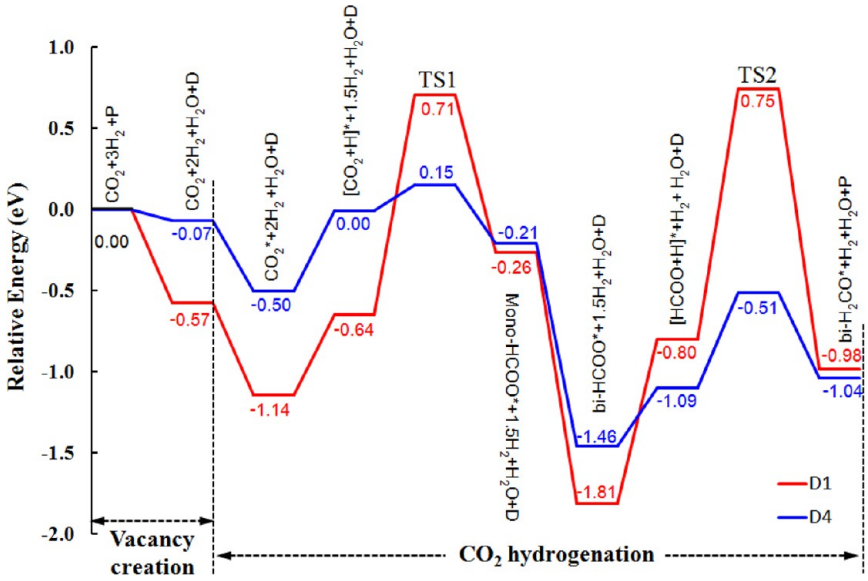

Figure 5. Potential energy profiles for the oxygen vacancy creation and first and second steps of CO_2 hydrogenation on the D1 and the D4 surfaces. Red line, D1 surface; blue line, D4 surface.

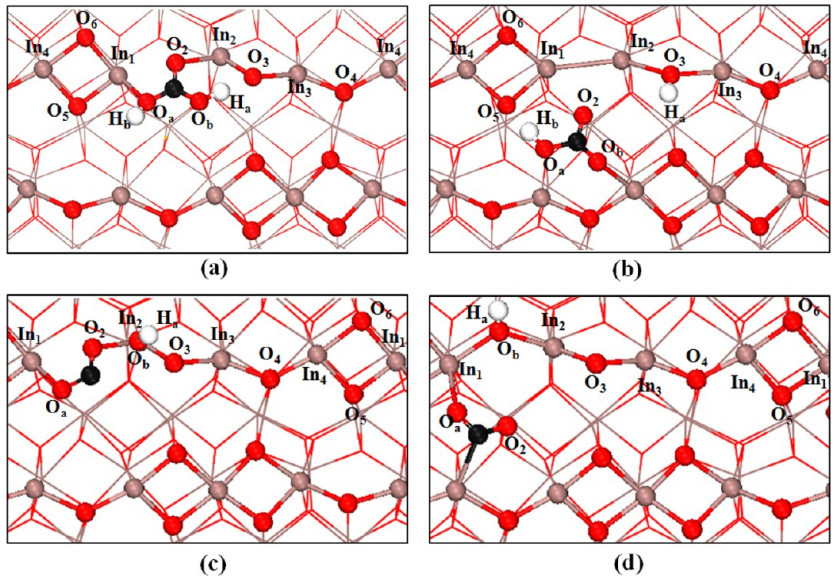

Figure 6. Initial and optimized structures of COHOH* (a and b) and (CO+OH)* (c and d) on the D1 surface.

favorable than that on D1. In general, the potential energy profile for CO_2 hydrogenation on D4 is smoother than that on D1.

On the other hand, the protonation product (COOH) of CO_2 could also be the intermediate for methanol formation from CO_2. We examined the possibility of hydrogenating COOH* to COHOH* and CO*+H_2O*on D1 and summarized the results in Figure 6. Figure 6a and b show the initial and optimized structures of COHOH*. In the initial structure, H_b was added to O_a of COOH*. Structural relaxation starting from this initial structure resulted in coadsorbed COOH and H_a, with COOH being migrated to the next chain, as shown in Figure 6b. This result indicates that COHOH is not a stable intermediate state and, therefore, is not likely to be the product state of COOH + H.

The structural feature of the In_2O_3(110) surface determined that direct hydrogenation of COOH to CO and H_2O is not possible. Instead, COOH needs to dissociate into CO and OH before OH reacts with coadsorbed H to form H_2O. Therefore, we examined the dissociation of COOH by breaking the C−O bond and placing OH on the neighboring In site, as shown in Figure 6c. Structural relaxation from this initial structure led to the stable structure shown in Figure 6d. In this structure, the artificially created CO in Figure 6c grabbed the O_2 atom from the surface and reformed CO_2, which bridges the two chains. The O_b from the OH fills in the vacancy left by O_2 and thereby repaired the chain structure. This result indicates that the COOH + H reaction does not lead to CO + H_2O.

On the D4 surface, the COOH* species is unlikely to form as CO_2 protonation needs to overcome a huge activation barrier (2.99 eV), excluding it as an intermediate for methanol formation on this surface. The surface hydroxyl formed on the surface as a result of heterolytic H_2 dissociation will disproportionate to form H_2O and desorb from the surface whereas the hydridic H_{In} will participate in the hydrogenation reactions. As such, we expect hydrogenation to be the dominant reaction on the D4 surface,

dx.doi.org/10.1021/cs400132a | ACS Catal. 2013, 3, 1296−1306

and formate formation on D4 is logically the key step leading to methanol on this surface. In the subsequent study, we analyzed the elementary steps leading to methanol formation on the D4 surface and mapped out the pathways of methanol synthesis from CO_2 hydrogenation.

3.3. Methanol Synthesis on the Oxygen Defective D4 Surface. As we discussed above, CO_2 hydrogenation to methanol is expected to follow the formate route on the D4 surface. The structural parameters and binding energies of reaction intermediates involved in the reaction are summarized in Table 3 with the structures shown in Figure 7. Figure 8

Table 3. Calculated Adsorption Energies, E_{ad} (eV), and Geometric Parameters of the Reaction Intermediates on the Perfect and the D4 Defective $In_2O_3(110)$ Surfaces

species	site	E_{ads}	bond length (Å)
H	in site	−2.77	$d_{(O-H)}$ = 1.75
	O site	−4.15	$d_{(In-H)}$ = 0.98
H_2	heter	−1.20	$d_{(In-H1)}$ = 1.72, $d_{(O-H2)}$ = 0.98
	homo	−0.44	$d_{(In-H1)}$ = 1.72, $d_{(In-H2)}$ = 1.73
H_2O	D4	−1.56	$d_{(In4-Ow)}$ = 2.09, $d_{(Ow-Ha)}$ = 0.98, $d_{(O-Hb)}$ = 1.00
CO	P	−1.40	$d_{(In3-C)}$ = 2.20, $d_{(In-O)}$ = 2.30, $d_{(C-O)}$ = 1.26, $d_{(C-O4)}$ = 1.30
CO_2	D4	−0.61	$d_{(In4-C)}$ = 2.20, $d_{(In3-Oa)}$ = 2.35, $d_{(In3-Ob)}$ = 2.24, $d_{(C-Oa)}$ = 1.25, $d_{(C-Ob)}$ = 1.30
mono-HCOO	D4	−2.43	$d_{(In3-Oa)}$ = 2.15, $d_{(C-Oa)}$ = 1.28, $d_{(C-Ob)}$ = 1.21, $d_{(C-H1)}$ = 1.20
bi-HCOO	D4	−3.68	$d_{(In3-Oa)}$ = 2.25, $d_{(In4-Ob)}$ = 2.23, $d_{(C-Oa)}$ = 1.26, $d_{(C-Ob)}$ = 1.29, $d_{(C-H1)}$ = 1.10
HCOOH	D4	−0.72	$d_{(In4-Ob)}$ = 2.31, $d_{(C-Oa)}$ = 1.33, $d_{(C-Ob)}$ = 1.25, $d_{(C-H1)}$ = 1.13, $d_{(Oa-H2)}$ = 0.99
mono-H_2CO	P	−0.57	$d_{(In3-Oa)}$ = 2.37, $d_{(C-Oa)}$ = 1.23, $d_{(C-H1)}$ = 1.11, $d_{(C-H2)}$ = 1.11
bi-H_2CO	P	−1.18	$d_{(In-Oa)}$ = 2.10, $d_{(C-Oa)}$ = 1.37, $d_{(C-Ob)}$ = 1.46, $d_{(C-H1)}$ = $d_{(C-H2)}$ = 1.11
H_3CO	P	−1.09	$d_{(In3-Oa)}$ = 2.13, $d_{(C-Oa)}$ = 1.40, $d_{(C-Ob)}$ = 1.46, $d_{(C-H1)}$ = $d_{(C-H2)}$ = $d_{(C-H3)}$ = 1.11
H_2COH	P	−2.38	$d_{(In3-Oa)}$ = 2.38, $d_{(C-Oa)}$ = 1.45, $d_{(C-Ob)}$ = 1.40, $d_{(C-H1)}$ = $d_{(C-H2)}$ = 1.11, $d_{(O-H3)}$ = 0.98
CH_3OH	P	−0.89	$d_{(In3-Oa)}$ = 2.29, $d_{(C-Oa)}$ = 1.44, $d_{(C-H1)}$ = $d_{(C-H2)}$ = $d_{(O-H3)}$ = 1.11, $d_{(O-H4)}$ = 1.00

summarizes the structures of initial, transition, and final states of each elementary step. The calculated reaction energies and activation barriers are given in Table 4.

3.3.1. Elementary Reactions Involved in CO_2 Hydrogenation to Methanol. H_2+P → H_2O+D4. According to this step, the D4 surface is treated as a product reducing the perfect surface with H_2. This dissociation of H_2 is spontaneous. Dissociative adsorption of H_2 on the perfect In_2O_3 surface forms one H−In bond and a hydroxyl group by combining with a lattice oxygen. The two species react to form a water molecule, which then desorbs from the surface. This step is slightly exothermic with a reaction energy of −0.07 eV. This step has been discussed in detail in our previous work.[26]

[CO_2+H] → mono-HCOO**. The adsorbed CO_2 reacts with the neighboring atomic H on In to form mono-HCOO on D4. As shown in Figure 8a, coadsorbed CO_2 and H in [CO_2+H]* is the initial state. In this state, CO_2 binds In_3 through O_a with a bond length of 2.41 Å, and H binds In_4 with a bond length of 1.74 Å. The reaction proceeds through H_1 approaching C. In TS1, the In_4-H_1 bond is stretched to 1.87 Å, and the distance between C and H_1 is 1.65 Å. The HCOO* binds In_3 in a monodentate configuration with a O_a-In_3 bond length of 2.15 Å. The reaction energy for this step is −0.21 eV, and the activation barrier is 0.15 eV. These results indicate that CO_2 hydrogenation to HCOO is both energetically and kinetically facile. The immediate product, i.e., mono-HCOO species, is not stable and will quickly transform to a more stable bidentate structure of HCOO*. The transformation is exothermic by −1.25 eV. The result is consistent with previous experimental observations and theoretical studies that the bi-HCOO species are dominant in methanol synthesis on many catalysts.[14,18,38,40−42] We note that similar activation barriers were reported for CO_2 hydrogenation on the Cu[14,15] and ZnO(0001).[18]

[HCOO+H] → bi-H_2CO*+$O_{surface}$.* HCOO had been suggested previously as the key reaction intermediate in methanol synthesis. In our calculation, hydrogenation reaction starts from [HCOO+H]* in which the H atom binds the In_4 site. The O_b-In_4 bond breaks, and the O_a-In_3 and O_b-In_3 bond lengths are 2.30 Å and 2.23 Å, respectively. In TS2, the In_4-H_2 bond is stretched to 1.91 Å, and the distance between the C atom and the approaching H atom is 1.50 Å. In the meantime, the O_b fills the oxygen vacancy O_{v4}, resulting in a similar configuration to that of H_2CO adsorbed on the perfect $In_2O_3(110)$ surface. In the final state [bi-H_2CO]*, the O_a atom binds In_3 with a bond length of 2.10 Å, and the C atom binds the O_b incorporated in the surface with a bond length of 1.46 Å. The reaction is almost thermally neutral with a reaction energy of +0.05 eV and an activation barrier of 0.57 eV. Compared to the HCOO hydrogenation on Cu surfaces,[13−15] the formate hydrogenation is more favorable on the $In_2O_3(110)$ surface, due to the fact that breaking the C═O bond of HCOO species is much easier on $In_2O_3(110)$ than on Cu. A low barrier (0.61 eV) for HCOO hydrogenation to H_2COO on the ZnO(0001) surface was also reported, and the reverse reaction, i.e. H_2COO dissociation, is barrierless.[18] Unlike the ZnO(0001) surface, the H_2COO species on $In_2O_3(110)$ is stable, and the dissociation barrier is 0.52 eV. The stability of H_2COO is key to the superior activity of the In_2O_3 catalyst toward methanol synthesis from CO_2 hydrogenation.

*[mono-H_2CO+H] → H_3CO**. H_3CO is the product of H_2CO direct hydrogenation. For reaction $H_2CO+H \rightarrow H_3CO$, bi-$H_2CO$ needs to be activated to mono-H_2CO first. This step costs 0.61 eV. We find that the coadsorption of mono-H_2CO and H_3 is very unstable, as the coadsorbed mono-H_2CO and H_3 reacts spontaneously during geometry optimization even for an initial H_3-C distance >3 Å. In order to stabilize the H_3 adatom, we added another H adatom on O_b, as shown in [mono-H_2CO +H_{In}+H]*. In TS3_1, H_3 approaches C with a H_3-C distance of 2.02 Å, and the distance between H_3 and In_4 becomes 2.38 Å. The formation of methoxy is exothermic by −0.60 eV with a barrier of 1.14 eV. For $H_2CO+H \rightarrow H_3CO$ on the D4 surface, two interesting observations are worth noting: (1) H_3 spontaneously binds with the C atom of mono-H_2CO forming CH_3O with no barrier, if there is no hydroxyl group between the mono-H_2CO* and the hydride H_3. (2) The coadsorbed bi-H_2CO and hydride, [bi-H_2CO+H_{In}]*, are not stable. The coadsorption state will decompose into the bi-HCOO* and gas-phase H_2 upon geometry optimization. A similar scenario has been previously observed on the Cu cluster.[14] These two observations clearly indicate that the D4 surface is very active for hydrogenation.

[bi-H_2CO+H] → H_2COH**. Another possible product is H_2COH from H_2CO protonation. Protonation of H_2CO to H_2COH starts at the coadsorbed bi-H_2CO and H_o, shown in [H_2CO+H_o]* in Figure 8d. In TS3_2, H_3 drifted away from O_3

dx.doi.org/10.1021/cs400132a | ACS Catal. 2013, 3, 1296−1306

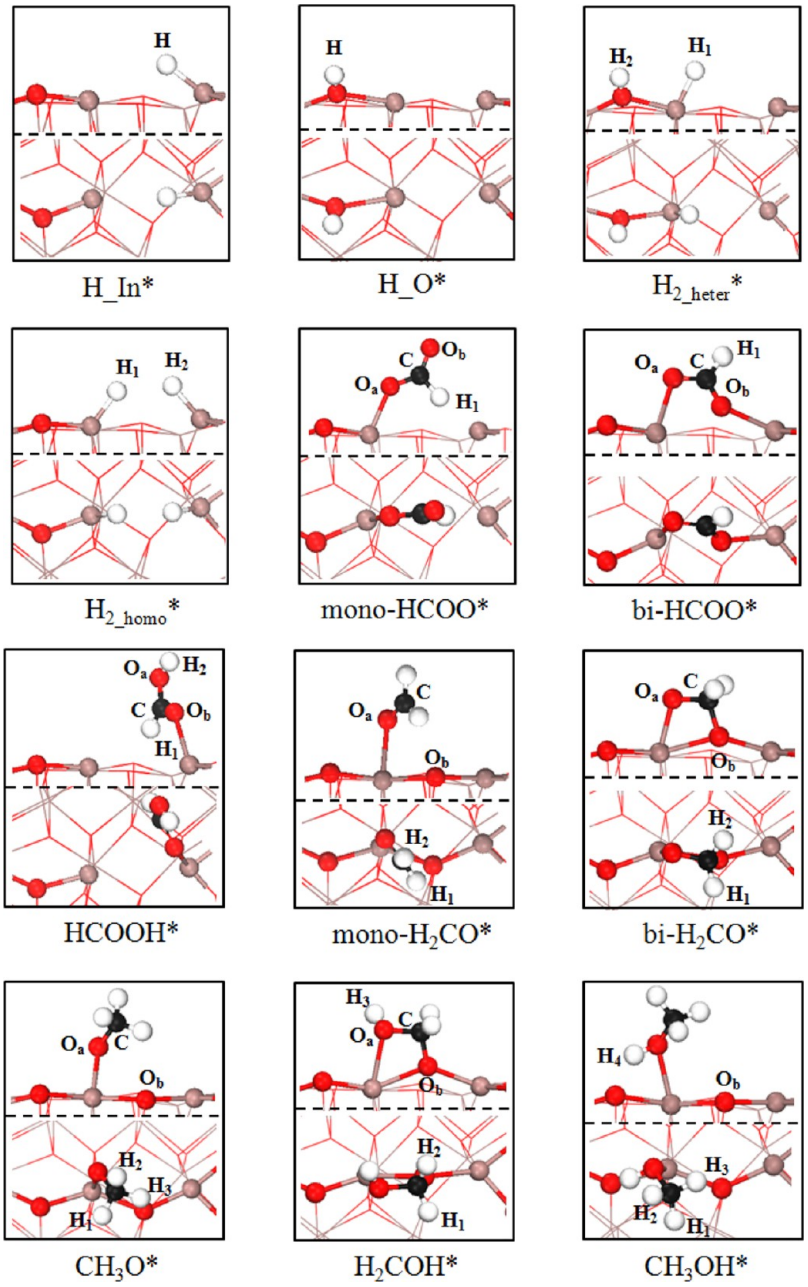

Figure 7. Optimized adsorption structures of the reaction intermediates involved in CO_2 hydrogenation to methanol on the D4 defective $In_2O_3(110)$ surface.

to 1.38 Å, and the distance between H_3 and surface O_a is 1.18 Å. The result shows that this step is endothermic by +0.83 eV and needs to overcome a barrier of 1.33 eV.

*[H_3CO+H]** → *CH_3OH**. One pathway leading to methanol formation is via H_3CO protonation. Prior to the reaction, the H_3CO'* species needs to rotate to a more stable configuration shown as [H_3CO+H]* with an energy gain of 0.27 eV. In this configuration, H_3CO* binds In_3 with a bond length of 2.13 Å, and the neighboring H_4 atom binds O_3. The protonation of H_3CO is initialized by H_4 stretching from O_a. In the transition state (TS4_1), the distance between H_4 and O_3 elongates to 1.40 Å, while the H_4-O_a forms a bond at a distance of 1.12 Å. The reaction energy of this step is +0.21 eV, slightly endothermic, and the activation barrier is 0.33 eV. Moreover, the activation barrier of methanol deprotonation is 0.12 eV. These results indicate that the protonation of methoxy and deprotonation of the adsorbed methanol are both facile and essentially reversible, similar to that on the ZnO(0001).[18] However, this is very different from that on the Cu surfaces where methanol deprotonation is less favorable than H_3CO protonation. The DFT calculated activation barriers for the H_3CO protonation on Cu (e.g., 1.17 eV[15] and 1.01 eV[13]) are much higher than that on the oxide surfaces. H_3CO protonation was considered to be the rate-limiting step on the Cu surfaces.

*[H_2COH+H]** → *CH_3OH**. Another pathway for methanol formation is via H_2COH hydrogenation. As shown in Figure 8f, the In_4-H_4 bond is 1.83 Å, and the distance between H_4 and C of H_2COH is 1.99 Å in the initial state [H_2COH+H_4]*. In the transition state (TS4_2), the H_2COH species is lifted up from the surface with the O_a-In_3 and $C-O_b$ bonds being 2.71 Å and 2.32 Å, respectively. Although the reaction is exothermic by −0.59 eV, the calculated activation barrier is 2.52 eV. This

dx.doi.org/10.1021/cs400132a | ACS Catal. 2013, 3, 1296−1306

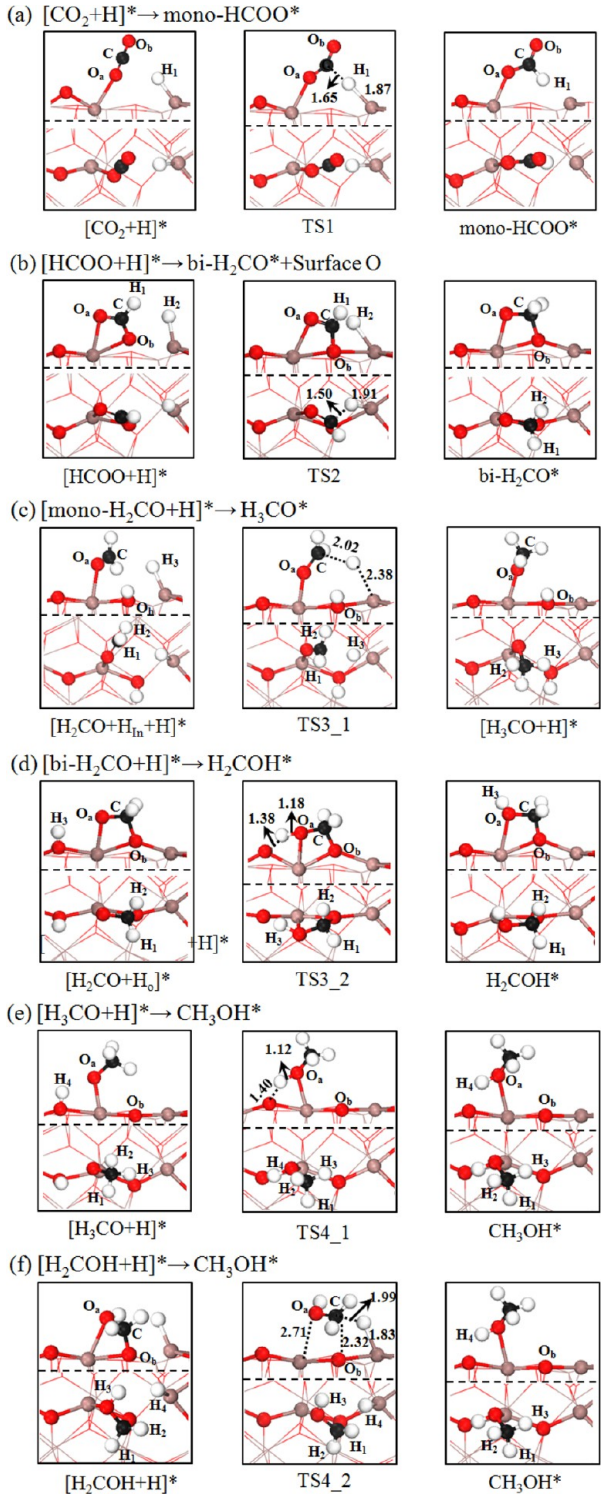

Figure 8. Elementary steps involved in CO_2 hydrogenation to methanol on the D4 defective $In_2O_3(110)$ surface. The corresponding bond lengths (Å) are shown in the figures.

extremely high barrier indicates that this hydrogenation step is kinetically prohibited. Again, this is similar to the case on the ZnO(0001) surface where the barrier is 1.66 eV[18] but totally different from the case on the Cu(111) surface where the barriers are only 0.51 eV[15] and 0.66 eV[13].

3.3.2. H_3CO Route vs H_2COH Route. In the above section, we discussed all elementary steps involved in two reaction pathways

Table 4. Calculated Reaction Energies, ΔE (eV), and Activation Barriers, E_a (eV), of Elementary Reaction Steps Involved in Methanol Synthesis from CO_2 Hydrogenation on the D4 Defective $In_2O_3(110)$ Surface

elementary reaction step	ΔE	E_a
$[CO_2+H]^* \rightarrow$ mono-HCOO*	−0.21	0.15
$[HCOO+H]^* \rightarrow$ bi-H_2CO^*+Surface O	+0.05	0.57
[mono-H_2CO+H]* → H_3CO^*	−0.60	1.14
[bi-H_2CO+H]* → H_2COH^*	+0.83	1.33
$[H_3CO+H]^* \rightarrow CH_3OH^*$	+0.21	0.33
$[H_2COH+H]^* \rightarrow CH_3OH^*$	−0.59	2.52

leading to the methanol formation from CO_2 hydrogenation on the D4 surface. The first pathway is via the methoxy (H_3CO) intermediate, following D4 + $2H_2$ + CO_2 → D4 + 3H + mono-HCOO → P + 2H + mono-H_2CO → P + H + H_3CO → P + CH_3OH. The second route is via the hydroxymethyl (H_2COH) intermediate; following D4 + $2H_2$ + CO_2 → D4 + 3H + bi-HCOO → P + 2H + bi-H_2CO → P + H + H_2COH → P + CH_3OH. The calculated potential energy surfaces for both reaction routes are shown in Figure 9.

At the onset, H_2 is used to reduce the perfect $In_2O_3(110)$ (P) surface to produce the defective surface with oxygen vacancy at the O_{v4} site (the D4 surface). Then, CO_2 adsorbs at the vacancy O_{v4} site. For CO_2 hydrogenation to mono-HCOO*, CO_2 needs to be activated by introducing the H adatom at the neighboring In site. This step is endothermic by +0.50 eV. Once CO_2 is activated, the hydrogenation occurs spontaneously. This hydrogenation step is both thermodynamically and kinetically favorable as the reaction is exothermic with a very small barrier of 0.15 eV. The mono-HCOO* is very unstable and quickly transforms to bi-HCOO* with large energy gain of 1.25 eV. The bi-HCOO* is activated by introducing a H atom in the neighboring In site, which needs an energy of 0.37 eV. By overcoming a barrier of 0.57 eV, bi-HCOO* is further hydrogenated to bi-H_2CO* and drops one of the O atoms into the vacancy O_{v4} site. Starting from the bi-H_2CO* configuration, both H_3CO and H_2COH intermediates could lead to methanol.

To form H_3CO, bi-H_2CO* needs to be activated to mono-H_2CO*, which is endothermic by 0.61 eV. Then mono-H_2CO* is hydrogenated to H_3CO by overcoming a barrier of 1.14 eV, and this step is exothermic by −0.60 eV. This is expected to be the rate limiting step, which has the highest barrier. Finally methanol forms via H_3CO* protonation by overcoming a barrier of 0.33 eV with an endothermicity of 0.21 eV. To form H_2COH, bi-H_2CO* is protonated by H_3 of the hydroxyl. This process needs to overcome a barrier of 1.33 eV with an endothermicity of +0.83 eV. The subsequent step, i.e., H_2COH* hydrogenation to methanol, is very difficult because of the huge barrier of 2.52 eV, although the step is exothermic by −0.59 eV. As such, the hydrogenation of H_2CO will lead to H_3CO, and H_3CO is the dominant intermediate for methanol formation. We also examined the HCOO + H → HCOOH reaction, which is endothermic by 1.38 eV. This value is much higher than that of the other elementary steps considered here. Therefore, the HCOO + H → HCOOH reaction was not included in the analysis.

3.3.3. Comparing CO_2 Activation on the In_2O_3 Surface and the Cu Surface. Adsorbed CO_2 on the D4 surface is highly activated, resulting in that CO_2 hydrogenation to HCOO* is both thermodynamically and kinetically facile. HCOO* hydrogenation to H_2CO needs to climb a barrier of 0.57 eV, and the

dx.doi.org/10.1021/cs400132a | ACS Catal. 2013, 3, 1296−1306

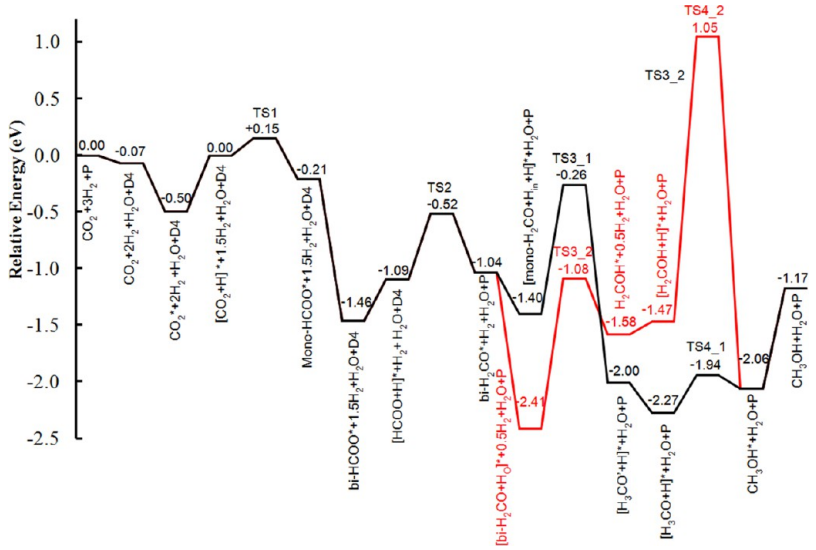

Figure 9. Potential energy surfaces for CO_2 hydrogenation to methanol on the D4 defective $In_2O_3(110)$ surface.

reaction is slightly endothermic. H_2COO is stabilized on the D4 surface through O replenishing the oxygen vacancy, forming H_2CO. Adding H to H_2CO hydrogenation could lead to two products: H_3CO and H_2COH. Methanol formation from the H_3CO protonation is more favorable than the H_2COH hydrogenation. The result is similar to that on ZnO(0001),[18] where a lower barrier for H_3CO protonation than for H_2COH hydrogenation was reported. However, Zhao et al. reported that methanol was the product of CO hydrogenation. In that case, CO_2 has to be reduced to CO first before being hydrogenated to methanol. Although HCOO and CO_3 were also found to form easily on the ZnO(0001) surface, these species only accumulate as spectators. In contrast, we find that the reverse water-gas reaction leading to the CO formation is strongly suppressed on the defective In_2O_3 surface. The adsorbed CO_2 will not be reduced to CO. Thus, CO_2, not CO, will be the major carbon source for methanol production on the defective In_2O_3 surface. In addition, we find that the oxygen vacancies on the In_2O_3 surface stabilize the critical intermediates involved in methanol synthesis, including HCOO, H_2COO, and H_2CO. In contrast, the H_2CO and H_2COO species are not stable on the Cu(111) surface.[13,15] In particular, the reaction $CH_3O + H \rightarrow CH_3OH$ step is extremely difficult with a barrier of 1.31 eV.[40] As a result, the In_2O_3-based catalysts would be advantageous over traditional Cu-based catalysts.

The key issue in the methanol synthesis from CO_2 hydrogenation is to break one of the C═O bonds. The breaking of the C═O bonds on Cu surfaces can only occur by dissociation intermediates such as H_2COOH ($H_2COOH \rightarrow H_2CO + OH$),[14,17,40] COHOH ($COHOH \rightarrow COH + OH$),[43] COOH ($COOH \rightarrow CO + OH$),[15] and HCOOH ($HCOOH \rightarrow HCO + OH$).[15] When oxide was introduced in the catalyst, as in the case of Cu/ZrO_2, CO_2 was found to split into CO and an O atom with a small barrier of 0.38 eV. However, the O species will poison the interface of Cu and ZrO_2.[40] For the In_2O_3 (or ZnO) system, the C═O bond cleavage is achieved by using one of the O atoms to fill the oxygen vacancy. This is much easier than that on the metal surface, as we demonstrated here. Therefore, we anticipate that the oxygen vacancies on the In_2O_3 surface play important roles in methanol formation from CO_2 hydrogenation. Methanol formation helps to repair the oxygen vacancy on the surface, while the H_2 in the reactive mixture helps to recreate the vacancies and, thereby, sustain the catalytic cycle.

4. CONCLUSIONS

Methanol synthesis from CO_2 hydrogenation on the In_2O_3 surface with an oxygen vacancy has been studied by using periodic DFT calculations. We established the relative stabilities of possible vacancy defects and chose the D4 surface to map out the reaction pathways for methanol formation. Two routes that share the same elementary steps, $CO_2 + H \rightarrow HCOO$ and $HCOO + H \rightarrow H_2CO + O_{surface}$, for CO_2 hydrogenation to methanol on the D4 surface were examined. Our results show that CO_2 hydrogenation to HCOO is both thermodynamically and kinetically favorable. The step for HCOO hydrogenation to H_2CO is slightly endothermic with a barrier of 0.57 eV. Subsequently, H_2CO hydrogenation to CH_3O is more favorable than protonation to the H_2COH for methanol formation. Our results demonstrate that the oxygen vacancy on the $In_2O_3(110)$ surface assists CO_2 activation and hydrogenation and also stabilized the key intermediates involved in methanol formation. In addition, methanol formation replenishes the oxygen vacancy sites whereas H_2 helps to generate the vacancies. The cycle between the perfect and defective states of the surface catalyzes the formation of methanol from CO_2 hydrogenation.

■ ASSOCIATED CONTENT

Supporting Information

A video of *ab initio* molecular dynamics simulations placing CO_2 in the vacancy site in the stable adsorption configuration. This material is available free of charge via the Internet at http://pubs.acs.org.

■ AUTHOR INFORMATION

Corresponding Author

*Tel.: 1-618-453-6406. E-mail: qge@chem.siu.edu.

Notes

The authors declare no competing financial interest.

■ ACKNOWLEDGMENTS

We gratefully acknowledge the support from the National Natural Science Foundation of China (#20990223) and from

U.S. Department of Energy, Basic Energy Science program (DE-FG02-05ER46231). D.M. was supported by the U.S. Department of Energy, Office of Basic Energy Sciences, Division of Chemical Sciences, Geosciences & Biosciences. The computations were performed in part using the Molecular Science Computing Facility in the William R. Wiley Environmental Molecular Sciences Laboratory (EMSL), which is a U.S. Department of Energy national scientific user facility located at PNNL in Richland, Washington.

REFERENCES

(1) Centi, G.; Perathoner, S. *Catal. Today* **2009**, *148*, 191−205.
(2) Song, C. *Catal. Today* **2006**, *115*, 2−32.
(3) Wang, W.; Wang, S.; Ma, X.; Gong, J. *Chem. Soc. Rev.* **2011**, *40*, 3703−3727.
(4) Waugh, K. C. *Catal. Today* **1992**, *15*, 51−75.
(5) Yang, Y.; Mims, C. A.; Mei, D. H.; Peden, C. H. F.; Campbell, C. T. *J. Catal.* **2013**, *298*, 10−17.
(6) Yang, Y.; Mims, C. A.; Disselkamp, R. S.; Mei, D.; Kwak, J.-H.; Szanyi, J.; Peden, C. H. F.; Campbell, C. T. *Catal. Lett.* **2008**, *125*, 201−208.
(7) Chinchen, G. C.; Denny, P. J.; Jennings, J. R.; Spencer, M. S.; Waugh, K. C. *Appl. Catal.* **1988**, *36*, 1−65.
(8) Askgaard, T. S.; Nørskov, J. K.; Ovesen, C. V.; Stoltze, P. *J. Catal.* **1995**, *156*, 229−242.
(9) Behrens, M.; Studt, F.; Kasatkin, I.; Kühl, S.; Hävecker, M.; Abild-Pedersen, F.; Zander, S.; Girgsdies, F.; Kurr, P.; Kniep, B.-L.; Tovar, M.; Fischer, R. W.; Nørskov, J. K.; Schlögl, R. *Science* **2012**, *336*, 893−897.
(10) Xu, L.; Mei, D.; Henkelman, G. *J. Chem. Phys.* **2009**, *131*, 244520−244528.
(11) Mei, D.; Karim, A. M.; Wang, Y. *J. Phys. Chem. C* **2009**, *115*, 8155−8164.
(12) Mei, D.; Xu, L.; Henkelman, G. *J. Catal.* **2008**, *258*, 44−51.
(13) Zhao, Y.-F.; Yang, Y.; Mims, C.; Peden, C. H. F.; Li, J.; Mei, D. *J. Catal.* **2011**, *281*, 199−211.
(14) Yang, Y.; Evans, J.; Rodriguez, J. A.; White, M. G.; Liu, P. *Phys. Chem. Chem. Phys.* **2010**, *12*, 9909−9917.
(15) Grabow, L. C.; Mavrikakis, M. *ACS Catal.* **2011**, *1*, 365−384.
(16) Bowker, M.; Hadden, R. A.; Houghton, H.; Hyland, J. N. K.; Waugh, K. C. *J. Catal.* **1988**, *109*, 263−273.
(17) Kiss, J.; Frenzel, J.; Nair, N. N.; Meyer, B.; Marx, D. *J. Chem. Phys.* **2011**, *134*, 064710−064714.
(18) Zhao, Y.-F.; Rousseau, R.; Li, J.; Mei, D. *J. Phys. Chem. C* **2012**, *116*, 15952−15961.
(19) Pan, Y.-x.; Liu, C.-j.; Ge, Q. *J. Catal.* **2010**, *272*, 227−234.
(20) Bielz, T.; Lorenz, H.; Jochum, W.; Kaindl, R.; Klauser, F.; Klötzer, B.; Penner, S. *J. Phys. Chem. C* **2010**, *114*, 9022−9029.
(21) Lorenz, H.; Jochum, W.; Klötzer, B.; Stöger-Pollach, M.; Schwarz, S.; Pfaller, K.; Penner, S. *Appl. Catal., A* **2008**, *347*, 34−42.
(22) Bielz, T.; Lorenz, H.; Amann, P.; Klötzer, B.; Penner, S. *J. Phys. Chem. C* **2011**, *115*, 6622−6628.
(23) Umegaki, T.; Kuratani, K.; Yamada, Y.; Ueda, A.; Kuriyama, N.; Kobayashi, T.; Xu, Q. *J. Power Sources* **2008**, *179*, 566−570.
(24) Chen, M.; Xu, J.; Cao, Y.; He, H. Y.; Fan, K. N.; Zhuang, J. H. *J. Catal.* **2010**, *272*, 101−108.
(25) Chen, M.; Xu, J.; Liu, Y. M.; Cao, Y.; He, H. Y.; Zhuang, J. H. *Appl. Catal., A* **2010**, *377*, 35−41.
(26) Ye, J.; Liu, C.-j.; Ge, Q. *J. Phys. Chem. C* **2012**, *116*, 7817−7825.
(27) Kresse, G.; Hafner, J. *Phys. Rev. B* **1993**, *48*, 13115−13118.
(28) Kresse, G.; Furthmüller, J. *Phys. Rev. B* **1996**, *54*, 11169−11186.
(29) Kresse, G.; Joubert, D. *Phys. Rev. B* **1999**, *59*, 1758−1775.
(30) Perdew, J. P.; Burke, K.; Ernzerhof, M. *Phys. Rev. Lett.* **1996**, *77*, 3865−3868.
(31) Blöchl, P. E. *Phys. Rev. B* **1994**, *50*, 17953−17979.
(32) Bader, R. F. W. *Acc. Chem. Res.* **1985**, *18*, 9−15.
(33) Henkelman, G.; Arnaldsson, A.; Jónsson, H. *Comput. Mater. Sci.* **2006**, *36*, 354−360.
(34) Henkelman, G.; Jónsson, H. *J. Chem. Phys.* **2000**, *113*, 9978−9985.
(35) Ueno, A.; Onishi, T.; Tamaru, K. *Trans. Faraday Soc.* **1971**, *67*, 3585−3589.
(36) French, S. A.; Sokol, A. A.; Bromley, S. T.; Catlow, C. R. A.; Rogers, S. C.; King, F.; Sherwood, P. *Angew. Chem., Int. Ed.* **2001**, *40*, 4437−4440.
(37) Tabatabaei, J.; Sakakini, B.; Waugh, K. *Catal. Lett.* **2006**, *110*, 77−84.
(38) Peng, G.; Sibener, S. J.; Schatz, G. C.; Ceyer, S. T.; Mavrikakis, M. *J. Phys. Chem. C* **2012**, *116*, 3001−3006.
(39) Pan, Y.-x.; Liu, C.-j.; Mei, D.; Ge, Q. *Langmuir* **2010**, *26*, 5551−5558.
(40) Tang, Q. L.; Hong, Q. J.; Liu, Z. P. *J. Catal.* **2009**, *263*, 114−122.
(41) Sotiropoulos, A.; Milligan, P. K.; Cowie, B. C. C.; Kadodwala, M. *Surf. Sci.* **2000**, *444*, 52−60.
(42) Fujitani, T.; Choi, Y.; Sano, M.; Kushida, Y.; Nakamura, J. *J. Phys. Chem. B* **2000**, *104*, 1235−1240.
(43) Yang, Y.; White, M. G.; Liu, P. *J. Phys. Chem. C* **2011**, *116*, 248−256.